THE JOURNAL OF PHYSICAL CHEMISTRY C
A JOURNAL OF THE AMERICAN CHEMICAL SOCIETY

pubs.acs.org/JPCC

Article

Ordered Chlorine Layer Formation from a Supersaturation of Chloroform

Ivan Soldo, Paul Schweer, Marvin Quack, Nico Knüfer, David Olivenza, Daniel P. Miller,* and Karina Morgenstern*

Cite This: https://doi.org/10.1021/acs.jpcc.4c04678

Read Online

ACCESS | Metrics & More | Article Recommendations | Supporting Information

ABSTRACT: The adsorption of ions on metallic surfaces is a powerful method to alter their electronic structure and thus tune their reactivity. A prominent example is chlorine on Ag(111). We investigate chlorine created by the room-temperature adsorption of chloroform on Ag(111) at supersaturation and the structures it forms from individual monomers to a full layer by using low-temperature scanning tunneling microscopy. The data is supplemented by temperature-programmed desorption and X-ray photoelectron spectroscopy after low-temperature adsorption under ultrahigh-vacuum conditions. Data interpretation is supported by density functional theory (DFT) calculations that account for dispersion forces. At low chlorine coverages, each chlorine locally alters the electronic structure of the surface. The adsorbed chlorine-induced local environment modification thereby creates preferential adsorption sites for other chlorines in their vicinity, stabilizing extended chlorine structures on Ag(111). Oligomer formation leads to distance-dependent cooperative effects of the charge transfer and thus impacts the electronic structure of the surface beyond the change by individual chlorines. At intermediate chlorine coverage, chlorine forms meandering chains with atoms adsorbed in alternating hcp and fcc hollow sites at distinct chlorine−chlorine distances. The one-dimensional structures convert to an open network at intermediate coverages and a two-dimensional hexagonal superstructure at saturation coverage. The DFT calculations suggest that the charge density extracted from the surface into the chlorines and the interaction between chlorine and silver atoms is improved as chlorines are adjoined closer at intermediate and high coverages.

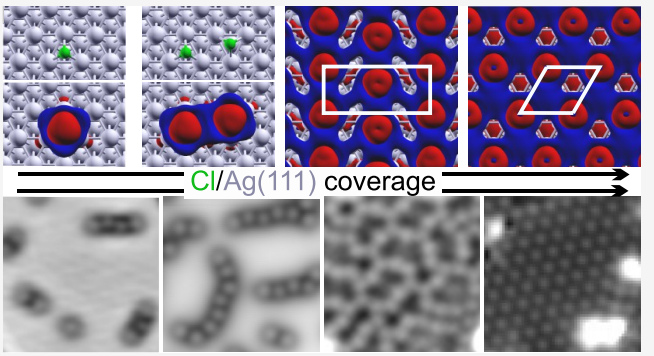

INTRODUCTION

The interaction of chlorine with Ag(111) has been of scientific interest because chlorine is a promoter in the partial epoxidation of ethylene to ethylene oxide on a silver catalyst under the industrial conditions of high pressure and temperature.[1] For a fundamental understanding of the promoting effect, chlorine is conventionally provided by chemical vapor deposition (CVD) to Ag(111). Chlorine is offered from the dissociative adsorption of ethylene dichloride,[2] Cl_2,[3] or tetrachloromethane (CCl_4).[4] For instance, molecularly adsorbed CCl_4 dissociates on annealing at 150 K and above.[5] The chlorine deposition was accompanied by the formation of tetrachloroethene, which desorbs and leaves no carbon trace on the surface.[5] Likewise, the dissociative adsorption of CCl_4 at room temperature yielded chemisorbed chlorine without carbon contamination on Ag(111).[6] Besides these achievements, very little is known about the chlorine adsorption under realistic reaction conditions, that is, ambient pressures and elevated temperatures, because these are far from the ultrahigh-vacuum (UHV) low-temperature conditions used in fundamental research. Moreover, the charge transfer to the chlorine oligomers and surface−adsorbate interactions have not yet been investigated on the local scale. It is thought to be responsible for the promoting effect of chlorine for reactions.

The main focus of fundamental research about chlorine on Ag(111) has been, so far, superstructure determination at close to monolayer coverage or above. A large structure variety exists, even under the defined UHV conditions. On Ag(111), the mobility of chlorine at low coverages and room temperature, supported by an estimated diffusion barrier of 100 meV,[6] hampers an unambiguous determination of its superstructure. Low-energy electron diffraction (LEED) demonstrated a compression from a low-coverage weak $\sqrt{3} \times \sqrt{3}$ $R30°$ superstructure.[3] For instance, the diffusive weak monolayer signal converts to a sharp $\sqrt{3} \times \sqrt{3}$ $R30°$

Received: July 12, 2024
Revised: October 31, 2024
Accepted: November 4, 2024

pattern below 180 K.[5] The pattern is most prominent at a Cl:Ag = 0.75 ratio.[5] It changes to a (5 × 5) superstructure at higher coverage.[7] Real-space investigations of Cl/Ag(111) revealed an even larger (17 × 17) superstructure of the monolayer at an interatomic distance of 0.41 nm.[8] Other reported Cl−Cl distances range from 0.41 nm to 0.50 nm.[3] The (17 × 17) superstructure persisted under extended further chlorine exposure.[8] With the improved spatial resolution available a decade later, the same group reported an incommensurate structure with a local (3 × 3) order at a slightly higher coverage involving a reconstruction of the Ag(111) surface.[9] Depending on the deposition parameters of additional chlorine, the (3 × 3) pattern coexists locally with Ag_3Cl_7 clusters[10] or more complex patterns at higher coverages.[11] The surface reconstructions provide the silver for the clusters.[10] Finally, low-temperature LEED reported a split-spot pattern with a (13 × 13) superstructure upon deposition from an in situ electrochemical cell.[12] Density functional theory (DFT) rationalized the variety of different superstructures by the lateral electrostatic repulsion of the charged chlorines[13] supported by complex and long-ranged interactions between the adsorbed Cl atoms.[6] Thermodynamically most stable is the $\sqrt{3} \times \sqrt{3}$ $R30°$ superstructure.[13] Indeed, different adsorption sites do not differ largely in energy at low coverage and other superstructures are similar in energy, e.g., the (2 × 2) at slightly lower coverage than the $\sqrt{3} \times \sqrt{3}$ $R30°$ superstructure.[13] The structure formation of the (2 × 2) superstructure is elucidated herein starting from well-separated monomers.

Further discrepancies exist for the adsorption energy and the charge state of chlorine on the Ag(111) surface. A desorption maximum for atomic chlorine at 870 K in temperature-programmed desorption (TPD) has been related to an adsorption energy of around 2.17 eV yet under assumptions that usually introduce large error bars.[3] It is smaller than the values calculated in the local density approximation (LDA) with Dirac−Slater exchange (3.73 eV)[14] or within the Ceperley−Alder version (3.61 eV).[15] The larger calculated value might result from the general overbinding trend of LDA. However, DFT-calculated values of 2.91 eV, 3.02 eV, and 3.09 eV with different DFT functionals are also larger than the experimental value.[15] Finally, the calculated charge of chlorine adsorbed in hollow sites varies from −0.2e in a Mulliken analysis[14] to −0.5e based on Löwdin charges.[13]

The variety of superstructures was attributed to an electrostatic repulsion of the partially charged atoms upon adsorption,[13] aided by a considerably flat potential-energy surface, similar to varying superstructures of cations on fcc surfaces.[16−18] Here, we explore this hypothesis for chlorine adsorbed from a supersaturation at room temperature on the local scale.

In this article, we first ensure that chloroform is a good candidate for purely chlorine layer formation on Ag(111) at room temperature by TPD from low-temperature chloroform adsorption and chemical information from low-pressure room-temperature adsorption by X-ray photoelectron spectroscopy (XPS). We then investigate the superstructure formation from single chlorines via submonolayer coverages to a monolayer from supersaturation at room temperature and how it affects the surface electronic structure in real space by using low-temperature scanning tunneling microscopy (LT-STM) and DFT which accounts for dispersion forces (DFT−vdW). By analyzing the interaction between individual chlorines, we rationalize the superstructure formation by chlorine-distance-dependent Ag−Cl interactions and cooperative charge transfer effects. DFT−vdW calculations that provide the bonding strength between atomic species show that the Ag−Cl interaction gets stronger with increasing chlorine coverage and when chlorine oligomers and chains form with chlorine atoms being approximately 0.45 nm apart. The study extends existing studies on chlorine adsorption on Ag(111) to the submonolayer range, important for understanding the interactions governing the superstructure formation, and to (near) ambient conditions, important for understanding the changes in reactivity of a Ag(111) surface upon adsorption of a charge withdrawing atom.

METHODS

The measurements were performed in two separate UHV chambers, one for LT-STM and TPD and one for XPS (base pressures: 2 × 10^{-10} mbar and 5 × 10^{-10} mbar). The two chambers host the same facilities for sample preparation.

In the STM/TPD chamber, Ag(111) is cleaned by repeated cycles of Ne^+ sputtering at 1.3 keV and ≈3 × 10^{-5} mbar, yielding a sputtering current of approximately 0.8 μA, for 30 min to 52 min and annealing at 830 K to 900 K for 25 min to 35 min until the amount of impurities detected in STM images is negligible.

In the XPS chamber, Ag(111) is cleaned by repeated cycles of Ar^+ sputtering at 1.3 keV and 3 × 10^{-6} mbar, yielding a sputtering current of 4 μA, for 10 min to 30 min and annealing at 850 K to 900 K for 10 min to 20 min. The surface cleanliness is confirmed by XPS.

The deuterated chloroform (trichloromethane, $CDCl_3$) is introduced into the UHV systems from the vapor pressure above the liquid, for the TPD and XPS or in liquid form from an Atomic Layer Injection (ALI) system for the LT-STM. The samples are positioned on a liquid helium (LHe, for TPD) or nitrogen (LN_2, for XPS) cooled manipulator for molecule deposition from the vapor pressure to face the opening of a dedicated molecule deposition chamber. They are placed on a transfer rod in a dedicated deposition chamber for depositions from a liquid drop at room temperature.

For CVD, the liquid is filled into a glass tube connected to the molecule deposition chamber by a leak valve. A pressure of 1 × 10^{-6} mbar or 1 × 10^{-5} mbar is set in the molecule deposition chamber for deposition for TPD or XPS, respectively, measurements before expanding the vapor into the main chamber toward the sample via a gate valve. It implies that the pressure at the sample is considerably lower, estimated to be about 2 orders of magnitude in previous work.[19,20] The chloroform is deposited for 21 s to 5 min (XPS: up to 17 h) at 43 K (room temperature). The monolayer formation time in the XPS chamber at room temperature is approximately 17 h, after which no further chlorine adsorbs. A deposition time of 4.5 h corresponds to around 0.27 ML.

The conversion efficiency of chloroform to chlorine on Ag(111) is low at room temperature, evident from the monolayer formation time of 17 h at approximately 1 × 10^{-7} mbar. A much higher chloroform pressure at the sample than in CVD is achieved by using the fast valve of an ALI system to introduce a droplet of chloroform to a UHV chamber, separated from the main chamber by a gate through valve. For this aim, 0.3 ml of chloroform is filled into the preinjection system of the ALI setup. The driving gas nitrogen pushes the

https://doi.org/10.1021/acs.jpcc.4c04678
J. Phys. Chem. C XXXX, XXX, XXX−XXX

liquid through a pulsed valve into the UHV system toward the sample. At a calculated adsorption energy of 40 meV, nitrogen does not adsorb on the Ag(111) sample at room temperature.[21] The chloroform is deposited with to ten pulses of 5 ms, leading to a maximum pressure reading of 1×10^{-3} mbar in the separated chamber. This value constitutes a lower value of the actual pressure at the sample due to the longer distance of the gauge than the sample to the pulsed valve. The pressure in the separated chamber is reduced for the lowest coverages by opening the gate-through valve between the molecule deposition chamber and the preparation chamber. In this case, the pumping of the molecule deposition chamber by a turbo molecular pump is supplemented by the ion pump of the preparation chamber. After deposition, the sample is transferred to an LHe-cooled manipulator with the cooling below 273 K within the cold shields of the LT-STM. It is placed on the LT-STM at 40 K. Measurements are performed at 7 K. Note that the ALI system is unsuitable for deposition on a precooled sample for TPD measurements because the high pressure it induces leads to major adsorption on the manipulator cooling system. The use of the ALI system is inhibited in the XPS chamber because of the sensitivity of the electron detector that is destroyed at high pressures.

TPD is performed at a heating rate of approximately 1 K/min. The desorption is monitored by a quadrupole mass spectrometer. The hot filament of the quadrupole mass spectrometer dissociates the chloroform. Thus, it is unknown whether the molecules were already dissociated at the surface. However, the similar temperature and shapes of the three observed peaks to earlier work[22] suggest that they are related to intact molecules leaving the surface. The dissociation products represent the intact molecules. They are recorded for a clearer TPD signal because the sensitivity of the quadrupole mass spectrometer is low at the m/z of the intact molecule.

The XPS measurements were carried out at 86 K using a Mg Kα X-ray source supplied with a power of 300 W. The binding energy was calibrated using the Ag $2p_{3/2}$ peak centered at 368.2 eV. The electrons are collected by a hemispherical analyzer (PHOIBOS 100 from Specs) at an angle normal to the surface and detected by a multichanneltron detector. The reaction is followed by monitoring the Cl 2p and C 1s XP regions. A Gaussian/Lorentzian product formula with a Shirley-type background was used for peak fitting. The only constraint for the Cl 2p peak fitting is their identical half width.

Periodic calculations were performed using the Vienna Ab initio Simulation Package (VASP)[23] with the optPBE-vdW[24,25] density functional, which accounts for London dispersion forces through an augmented nonlocal correlation functional. For brevity, they are named DFT−vdW. The addition of London dispersion forces is necessary to studying adsorption at metallic surfaces, where weak long-range interactions play a significant role. A plane-wave basis set energy cutoff of 500 eV was used in the geometry optimizations and single-point computations. The projector augmented wave method[26,27] was used to treat the core states, as implemented within VASP. A Γ-point centered $3 \times 3 \times 1$ Monkhorst−Pack[28] K-grid was used in all periodic calculations adsorbed to the Ag(111) surface and in the gas phase, respectively. All atoms were allowed to relax fully within the surface−adsorbate systems in the geometry optimizations, except for the bottom two layers of the three-layer Ag(111) surfaces, which were kept fixed at the optPBE-vdW computed bulk lattice constant for Ag, which results in Ag−Ag bond lengths of 0.295 nm.

Single-point calculations on optimized structures were performed to obtain work functions, Bader charges, charge densities, charge density difference (CDD) isosurfaces, and simulated STM images. Simulated STM images were calculated using the Tersoff−Hamann approximation[29] by measuring specific local density of states above the Fermi level of the surface−adsorbate system using voltages of 1.2 V and 1.5 V at simulated STM tip heights positioned 0.42 nm above the top layer of the Ag(111) surface. The CDD isosurfaces were calculated by subtracting the clean Ag(111) surface charge density and each individual chlorine atom charge density from the total Ag(111)−chlorine system surface−adsorbate charge density. The red and blue CDD isosurfaces indicate charge gain and loss, respectively. Plane-averaged CDD (PACDD) and work function plots were computed by averaging the z-direction CDD and potential. The PACDD plots provide more information about charge than the Bader charges because the PACDD captures the full influence of adsorption by accounting for the charge displacement due to influences such as Pauli repulsion, dispersion, charge transfer, and bonding by relating the clean Ag(111) surface and free chlorine atom to the Cl−Ag(111) chemisorbed structure. The PACDD shows the e/nm values in the entirety of the surface−adsorbate model from the Ag(111) surface to the space between the surface and the adsorbate to the adsorbate. Changes in the work function were computed to observe the impact of chlorine chemisorption on the Ag(111) surface.

The integrated crystal orbital Hamilton population (iCOHP) and integrated crystal orbital overlap population (iCOOP) values were computed using a local-orbital basis suite toward electronic structure reconstruction.[30] An iCOHP value provides the energetic strength of a bond or interaction between two atoms. An iCOOP value provides the bond order for the two atoms. A negative iCOHP value is indicative of stability and is favorable. A positive iCOOP value indicates bonding, whereas a negative iCOOP value indicates antibonding. The iCOHP and iCOOP calculations were performed by using only the top layer of the surface in the chlorine−Ag(111)-optimized surface-adsorbed models.

The unit cell dimensions used for all of the calculations were 1.772 nm × 1.535 nm × 3.000 nm, with all three axes being large to ensure sufficient vacuum space to prevent unwanted periodic interactions in the z direction and between adsorbed chlorine structures in the x and y directions. The unit cell dimensions for the Ag(111) surface were kept the same except in two of the superstructure models. In the site 5 and site 7 superstructure models, the unit cell dimensions were 1.181 nm × 1.535 nm × 3.000 nm, and in the site 6 and site 6 superstructure models, the unit cell dimensions were 1.772 nm × 1.023 nm × 3.000 nm.

The work function of the Ag(111) surface is reported to be (4.72 ± 0.02) eV experimentally,[31] which is in good agreement with the work function of the Ag(111) surface computed at 4.71 eV using the 1.772 nm × 1.535 nm × 3.000 nm unit cell and 4.73 eV using the 1.181 nm × 1.535 nm × 3.000 nm unit cell.

Adsorption energies (E_{ads}) were computed on a variety of chlorine structures, sites, and coverages with the following equation:

$$E_{ads} = E_{surf+nCl} - nE_{Cl} - E_{surf} \quad (1)$$

where the optimized Ag(111)−chlorine system ($E_{surf+nCl}$), gas-phase chlorine atom (E_{Cl}) multiplied by the number of

https://doi.org/10.1021/acs.jpcc.4c04678
J. Phys. Chem. C XXXX, XXX, XXX−XXX

chlorine atoms (n), and clean optimized Ag(111) surface (E_{surf}) energies were used. When the adsorbate was not chlorine, the following adsorption energy equation was used:

$$E_{ads} = E_{surf+ads} - E_{ads} - E_{surf} \quad (2)$$

where the optimized Ag(111)−$CDCl_3$, Ag(111)−C_2Cl_4, Ag(111)−D, and Ag(111)−D_2, adsorbate, and clean optimized Ag(111) surface energies were used. Larger values in magnitude of E_{ads} correspond to stronger adsorption. In certain instances, the adsorbate energy used for calculating the adsorption energy for hydrogen was half of the D_2 gas-phase energy. The Cl, Ag, C, and H atoms are colored green, white, gray, and white/black, respectively.

RESULTS AND DISCUSSION

To set the stage, we recall that the 3-fold rotational symmetry of deuterated chloroform ($CDCl_3$) around its D−C bond matches the symmetry of the Ag(111) surface. This notion is supported by DFT−vdW calculations. In its preferred adsorption site, the deuterium points away from the surface and the carbon atom levels above an fcc site. The chlorine−chlorine distance of 0.295 nm matches the calculated Ag−Ag distance of 0.297 nm, allowing the three chlorines to interact in atop sites directly with the three surface atoms at a typical physisorption distance of 0.318 nm (Figure 1a, inset). The symmetry and distance fit matches make chloroform a good source of chlorine on Ag(111). Each chloroform could potentially release three chlorines.

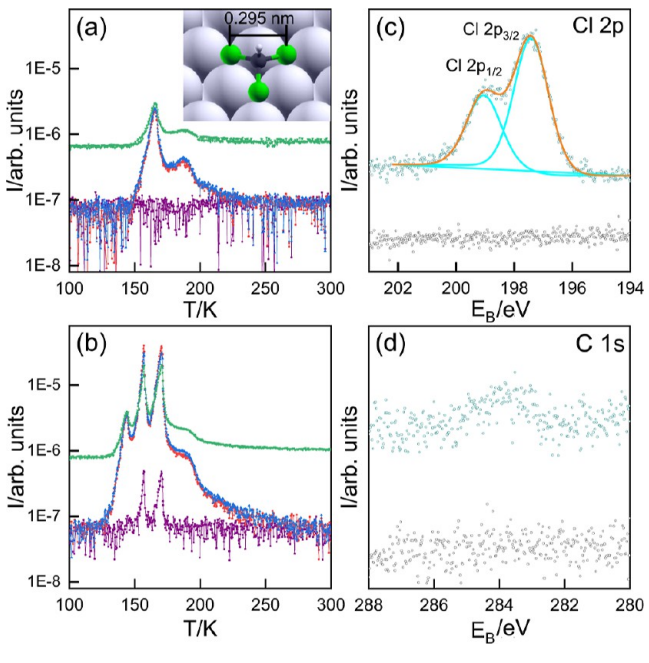

Figure 1. Chlorine adsorption on Ag(111) from chloroform: (a,b) TPD after (a) 0.2 and (b) 1 L adsorption at 43 K; m/z = 35 (Cl), m/z = 47 (CCl), m/z = 84 ($CDCl_2$), and m/z = 119 ($CDCl_3$) signals in green, blue, red, and purple, respectively; see experimental methods for the origin of the dissociation products; (c,d) XPS before (gray symbols) and after (cyan) exposure to chloroform for 17 h at room temperature yielding a 1 ML coverage: (c) Cl 2p region with double fit (cyan) and its sum (orange) and (d) C 1s region; inset in (a): Calculated chloroform adsorption structure with the Cl-to-Cl distance provided.

We employed temperature-programmed desorption (TPD) and X-ray photoemission (XPS) to ensure that the room-temperature deposition of chloroform yields chlorine and not chloroform. At a relatively weak calculated adsorption energy of 0.455 eV, chloroform is expected to adsorb transiently at room temperature. It is confirmed by TPD data echoing published data qualitatively (Figure 1a,b). As detailed in the Methods section, the dissociation products are created after desorption from the surface in the mass spectrometer and do not reflect dissociated species on the surface. In the earlier work, peaks at around 140 K, 150 K, and 170 K were assigned to the chloroform multilayer, bilayer, and monolayer, respectively.[22] After 0.2 L of adsorption, the monolayer peak is at a slightly lower value of 165 K (Figure 1a). After 1 L adsorption, the multilayer, bilayer, and monolayer peaks agree well with the earlier work, at 144 K, 157 K, and 171 K, respectively (Figure 1b). The slight difference in temperature is attributed to the difference in setup, heating rate, and the general uncertainty of thermocouples of around 5 K. A tail beyond the monolayer peak, existing at all investigated coverages, was not discussed in ref 22. It peaks for 0.2 L at 187 K and mostly vanishes at 210 K. The tail peaks for 1 L also at 187 K and vanishes at around 230 K. We assign it tentatively to desorption from defect sites, e.g., step edges. Overall, the TPD data confirm that the intact chloroform does not stick to the surface at room temperature.

Indeed, there is no indication of chloroform in the XPS data after room-temperature adsorption. However, there is also no indication of chlorine adsorption in the XPS data after short exposure times at room temperature. Only an extended exposure to the chloroform vapor leads to a single doublet in the XP spectrum in the Cl 2p range (Figure 1c). The peaks centered at 199.0 and 197.4 eV correspond to the Cl $2p_{1/2}$ and Cl $2p_{3/2}$ orbitals for chlorine bonded to Ag.[32] The bond is of ionic character.[15] The absence of peaks at higher binding energies, indicative of C−Cl or D−Cl bonds, demonstrates that neither chloroform is adsorbed on Ag(111) at room temperature nor does it react to surface-adsorbed D−Cl. The absence of chlorine bonded to carbon is consistent with the TPD data and the calculated adsorption energy of 0.455 eV of chloroform in its preferred adsorption geometry with the carbon residing above an fcc hollow adsorption site and the chlorines above atop sites (Figure 1a, inset). The absence of chlorine bonded to deuterium is expected as the desorption temperature of HCl from Ag(111), closely related to the possible reaction product DCl (cf., the similar adsorption energies of $CHCl_3$ and $CDCl_3$ presented in the Supporting Information), is slightly above 100 K.[33] Likewise, atomic or molecular deuterium desorbs far below room temperature with associative desorption from Ag(111) below 180 K,[34] consistent with our DFT−vdW calculations, yielding a minute adsorption energy of only 0.058 eV for H_2 or D_2 in the favored bridge adsorption site (see Supporting Information).

In addition, there are only trace amounts of carbon, evidenced by a broad peak at 283.9 eV with a low intensity (Figure 1d). We relate the traces of carbon to a small amount of impurities at the step edges after the deposition with the ALI system (not shown). Chloroform (0.46 eV) binds much weaker than chlorine does (3.32 eV, according to our calculation). Therefore, chlorine is expected to persist on Ag(111) at high temperatures. XPS and DFT−vdW thus unambiguously confirm that the dissociative adsorption of

https://doi.org/10.1021/acs.jpcc.4c04678
J. Phys. Chem. C XXXX, XXX, XXX−XXX

$CDCl_3$ on Ag(111) leads to the formation of negatively charged chlorines.

Having confirmed that chloroform is a suitable source of chlorine, we turned to its adsorption under the higher-pressure conditions provided by the ALI system and how it influences the electron distribution on the surface. Circular depressions surrounding protrusions are scattered across the surface at submonolayer coverages (Figure 2).[35,36]

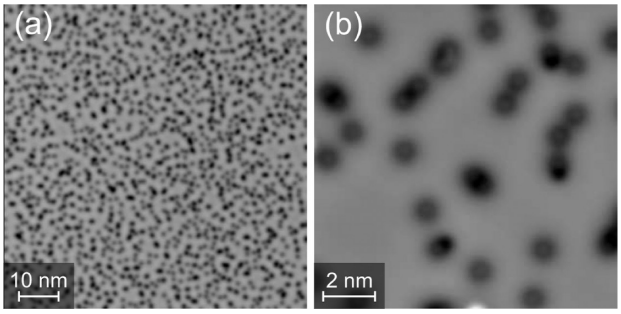

Figure 2. Chlorine adsorption on Ag(111): (a,b) STM images at two different scales; the sample was prepared by one pulse from the ALI system; the images were recorded at (a) 197 mV, 28 pA and (b) 312 mV, 510 pA.

We assign the smallest feature to the monomer based on the long history of STM imaging of individual adsorbed atoms as circular protrusions of around 1 nm in diameter.[37,38] The monomers adsorb preferentially in hollow sites with a slight preference for fcc (3.317 eV) over hcp (3.305 eV) adsorption, according to our DFT−vdW calculations (Figure 3a), in qualitative agreement with earlier studies[14] and consistent with an experimentally determined hollow site adsorption.[39]

The apparent depression implies that the local density of states is decreased from that of the Ag(111) surface; i.e., the adsorption induces a charge transfer from the Ag(111) surface to the chlorine. It is consistent with a charge transfer to the chlorine calculated earlier[13,14] and supported by DFT−vdW calculations that provide a Bader charge for chlorine of $-0.53e$, in fair agreement with earlier results that yielded $-0.51e$ on a smaller 3×3 simulation cell.[15] The slightly smaller charge at a smaller simulation cell size is consistent with a smaller charge at higher coverage for our larger simulation cell (see Supporting Information). A PACDD plane−averaged charge density difference (PACCD) calculation reveals that the charge accumulation in the plane of the chlorine reaches as much as 30.21 e/nm, while the Ag loses 64.12 e/nm for the monomer on Ag(111) (Figure 3j,k, black line). The CDD isosurfaces for the monomer display a large charge gain at the chlorine (Figure 3b, red) and loss from the Ag surface (blue). The significant charge gain at the chlorine and the significant charge loss on top of the Ag(111) surface surrounding the chlorine support the dark depression surrounding the chlorine in the experimental STM imaging, qualitatively reproduced in the simulated STM image (Figure 3c). The blue region is far broader than the size of the chlorine at small isovalues. Also, in experiment, the influence of the monomer on the surface charge density extends much further than its van-der-Waals size, to around 1 nm around its center.

An electronic origin of the image formation results from apparent height spectroscopy.[42] The weak protrusions within the apparent depressions change to brighter protrusions at around 1.3 V and even brighter protrusions at 1.8 V (Figure 4). A voltage-dependent imaging is reproduced in simulated STM images. In particular, the apparent height of the chlorines increases appreciably when going from 1.2 V (Figure 4, left inset) to 1.5 V (Figure 4, right inset), reflecting perfectly the images recorded at 1.3 and 1.8 V, respectively. A small deviation in absolute voltage is attributed to the imprecision in DFT in band gap determination.

A charge on the chlorines is corroborated experimentally by a strong variation in the local density of states visible at small voltages as protruding regions for the surfaces between the chlorines (Figure 5a). Such voltage-dependent changes were attributed earlier to standing waves of electrons in the Ag(111) surface state that develop between objects that scatter the electrons.[40] Here, the chlorines are the scattering centers, but their mutual distance is too small to support the full electron wavelength. Thus, not a full standing wave pattern develops but an increase in local density of states at the middle between the scattering centers, similar to surface electrons confined between step edges at a small distance.[41]

The apparent depths of depressions far away from others are distinctly smaller than those in the proximity to others. Different apparent depths suggest that the charge transfer is distance-dependent. It is corroborated by pushing the chlorines of different apparent heights laterally toward each other, leading to a 10-fold increase in local coverage. The differently imaged species adapt to the same appearance (Figure 5b). A decrease in the Cl 2p binding energy by increasing the coverage from around one-fourth to a full monolayer is indicative of a change in the charge state (Figure 5c). Thus, the direct environment of the chlorine influences how it is imaged and, consequently, what the charge state is.

We analyzed dimers at various distances to confirm the cooperative charge transfer experimentally. The imaging of the chlorine pairs depends on their distance. Two chlorine monomers at distances of 1.8 nm or more are identical to two single monomers, the surface reaching its overall value between them (Figure 6a,b). In contrast, the apparent height between the two chlorine monomers decreases at closer distances. At a distance of 1.4 nm, approximately five atomic distances in the Ag(111) surface, it remains −4 pm below the surface value (Figure 6c,d). At a distance of 1.1 nm, i.e., approximately four atomic distances, it stays approximately −9 pm below the value of the protrusions above the chlorines (Figure 6e,f). At closer distances, the apparent height decreases grandly to approximately −18 pm at a 0.95 nm distance, i.e., 3a with the lattice constant of Ag(111) (Figure 6g,h), and −27 pm at 0.6 nm (2a, Figure 6i,j). It is approximately three times the apparent depth of the monomers, thus, not simply the superposition of two charge transfers. This distinct depression is reproduced in the STM image calculation (Figure 3f). The dependence of apparent depths on the chlorine−chlorine distance confirms the strong surface-mediated interaction, a cooperative effect leading to more charge transfer to a pair of closely spaced than two well-separated chlorines. It is consistent with the different charge states calculated at different chlorine densities (see Supporting Information).

A dependence of the charge state on the chlorine distance is corroborated by Bader charge analysis and PACDD calculations (Table 1). The Bader charge on the chlorine decreases slightly as coverage increases from the monomer ($-0.53e$), dimer ($-0.52e$), and trimer ($-0.51e$) to the superstructure ($-0.49e$; Table 1). However, the PACDD plots display a larger charge density accumulation on the chlorine, implying that

https://doi.org/10.1021/acs.jpcc.4c04678
J. Phys. Chem. C XXXX, XXX, XXX−XXX

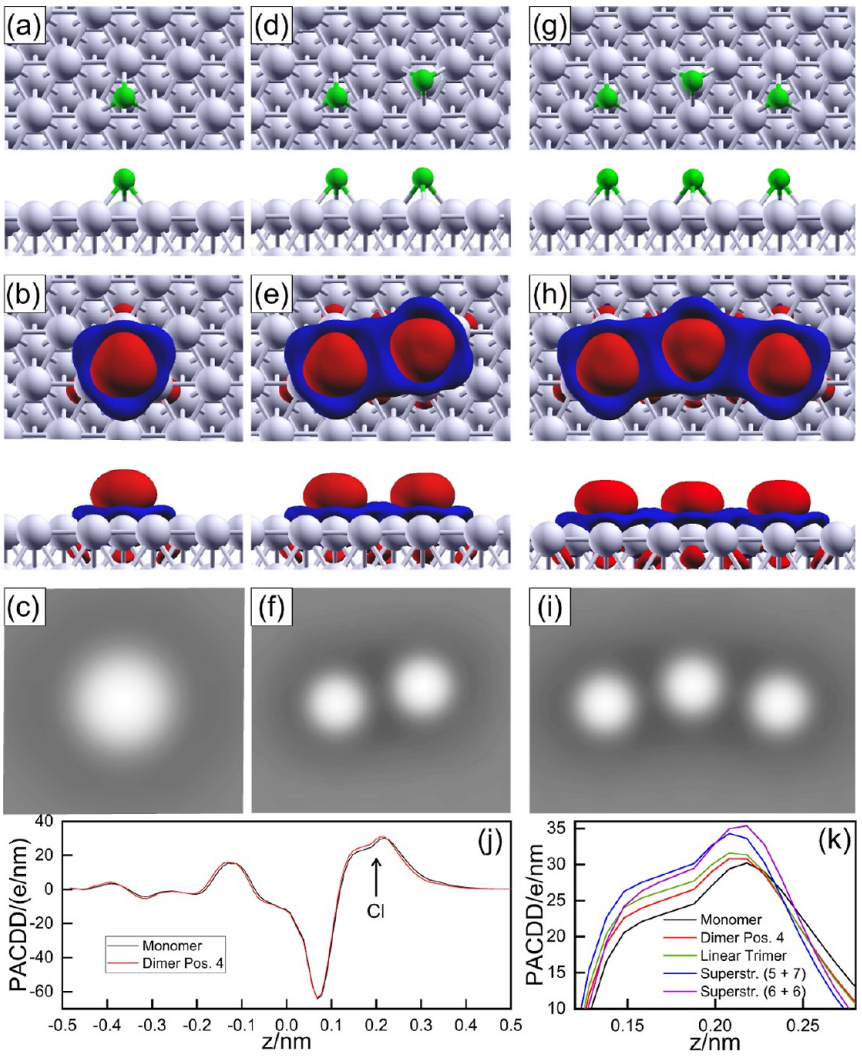

Figure 3. Charge transfer of chlorines to Ag(111): (a−c) monomer and (d−f) dimer in adsorption site 4 and (g−i) linear trimer; (a,d,g) optimized structures in top and side view; (b,e,h) CDD isosurfaces at an isovalue of ±5.0 e/nm^3 with charge gain in red and charge loss in blue in top and side view; see Supporting Information for a higher isovalue; (c,f,i) simulated STM images on a nonlinear gray scale at 1.2 V; see Supporting Information for the same images on a linear gray scale; (j,k) PACDD of chlorine on the Ag(111) surface perpendicular to the surface plane at z = 0 nm: (j) full z range for the monomer (black) and the dimer (red) and for other oligomers, see Supporting Information, and (k) selected adsorbed chlorine region for the monomer (black), dimer (red), linear trimer (green), quasi-hexagonal superstructure (blue), and hexagonal superstructure (purple).

packing of the chlorines betters the ionic interaction with the underlying Ag(111) surface (Figure 3j,k, black line). Moreover, the charge density accumulation on chlorine increases with increasing chlorine coverage (Table 1). When more chlorines are added to the Ag(111) surface, the PACDD shows a greater sum of e/nm gain in the chlorines and loss at the Ag(111) surface (Figure 3k and Table 1).

We characterize differently sized oligomers to further understand the mutual effect of the chlorines on charge transfer (Figure 7a). The monomer M exhibits a sombrero shape, a protrusion within an apparent depression (Figure 7b). At 12 mV, its maximum is around −7 pm below the surface, surrounded by a concentric dark ring of −8 pm, a minor difference of only 1 pm between the protrusion in the middle of the hole and the rim around it (Figure 7c). The sombrero shape reflects the charge transfer from the Ag surface (blue) to the negatively charged chlorine (red), as visualized in the CDD plots (Figure 3b).

The dimer D is imaged as a double sombrero-shaped adsorption structure with its distinct depression between the two monomers from the cooperative effect of the charge transfer (Figure 7a,d). It results from the charge transfer from the surface to the chlorines (Figure 3e,j,k, red line). The dimers exist in varying orientations.

An appreciable depression exists likewise between the individual protrusions of more extended structures, trimers T and rare tetramers TT (Figure 7a). The long axes of linear trimers or tetramers follow approximately one of the Ag(111)−⟨110⟩ directions in a zigzag fashion. The zigzag results from alternating fcc/hcp sites of linear trimers (Figure 3g). The depression between them is related to the charge transfer from the silver surface (blue) to the chlorine (red) in the CDD plot (Figure 3g) and is reflected in the calculated STM image (Figure 3i). Other trimers are angled (T_A in Figure 7e) or form a triangle (T_T in Figure 7e). Indeed, the linear (T_L) and angled trimer (T_A) are almost isoenergetic with the energetically preferred triangular trimer (T_T), all being more stable than separated monomers (Table 2, see Supporting Information for the calculated structures).

https://doi.org/10.1021/acs.jpcc.4c04678
J. Phys. Chem. C XXXX, XXX, XXX−XXX

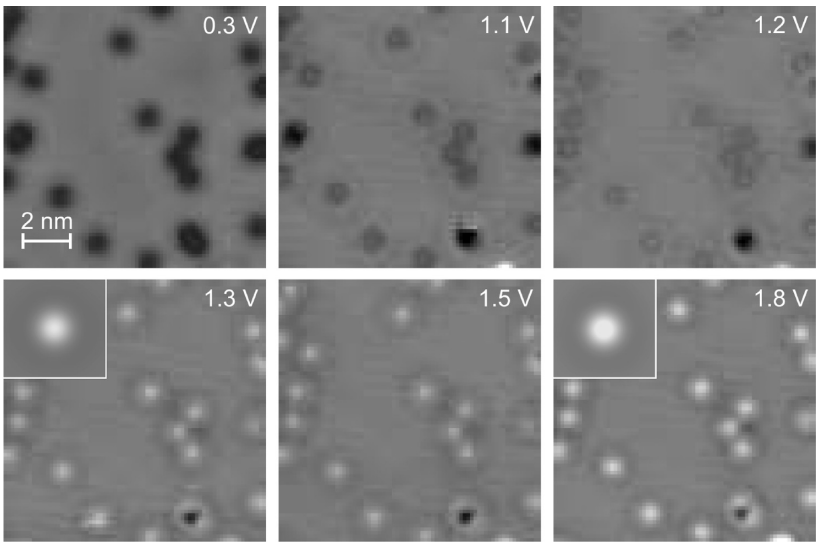

Figure 4. Voltage dependence of imaging: STM images at indicated voltages; the tunneling current is 0.27 nA; the insets represent simulated images at 1.2 V (left) and 1.5 V (right) of a monomer (not to scale); the sample was prepared by one pulse from the ALI system.

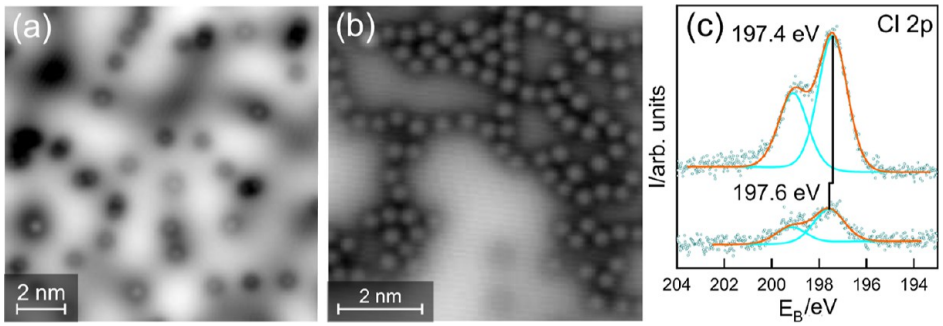

Figure 5. Influence of chlorine density on charge transfer: (a,b) STM images at a small bias voltage after adsorption (a) and after pushing the chlorines together (b); the sample was prepared by one pulse from the ALI system; (c) XPS Cl 2p region after exposure to chloroform for 4.5 h (bottom, 0.27 ML) and 17 h (top, 1 ML) at room temperature with double fits (cyan) and their sum (orange); the images were recorded at (a) 10 mV, 82 pA and (b) 5 mV, 60 pA.

The formation of the oligomers from negatively charged species is unexpected at low coverages, where the chlorines could maximize their distance to reduce electrostatic repulsion. We discuss the interaction between two chlorines for understanding the formation of the oligomers. Relative to its most favorable adsorption site on Ag(111), the fcc hollow site, the electrostatic repulsion between charged chlorine atoms at distances below 0.39 nm hinders the adsorption of a second chlorine in the neighboring 3-fold hollow sites marked 1−3 in Figure 8a, top, while at larger distances, the potential is reminiscent of a Lennard-Jones potential, approximated as a dotted line in Figure 8a. The adsorption energies in the repulsive part of the potential are less than those of two well-separated chlorines (Table 2). Chlorines in dimers at sites 1 and 2 are even displaced from their preferred hollow site due to the repulsion (Figure 8b,c). Indeed, dimers at distances corresponding to sites 1−3 do not exist in experiment. According to our DFT−vdW calculation, the adsorption energy for a second chlorine at sites 4 to 7 is more stable than the adsorption energies of two individual chlorines on Ag(111). Thus, negatively charged chlorines seemingly attract each other at site 4 at 0.45 nm, site 5 at 0.50 nm, site 6 at 0.58 nm, and site 7 at 0.60 nm (Figure 8a), leading to dimer distances of 0.45, 0.50, 0.59, and 0.62 nm for the calculated dimer 4 (Figure 8e), dimer 5 (Figure 8f), dimer 6 (Figure 8g), and dimer 7 (Figure 8h), respectively (Table 2). The gain in adsorption energy is tentatively explained by a more efficient charge transfer to a dimer at these distances than to the separated monomers, supported by the PACDD (Figure 3j,k) and an increased Ag−Cl interaction revealed by the iCOHP calculations (Table 2).

As seen in Tables 1 and 2, when chlorines are brought to being 0.45 nm apart, being the site 4 dimer, from smaller or larger distances, the adsorption energy grows more stable due to the dimer at site 4 having the largest in magnitude iCOHP value of −6.470 eV/Cl. In this hollow site, chlorine interacts with three Ag atoms. The iCOHP values provide the bonding strength between two atoms of a system, where a negative value is indicative of favorability. The gain in stability through iCOHP detailed bonding strength is profound when increasing the distance to the dimer in site 4 adsorption but subtle, yet present, when decreasing from the dimer in site 7 to the preferred dimer in site 4. The PACDD values show that the dimer in site 4 relative to the other dimers has the largest charge density gain within the substrate, the lowest charge loss just above the Ag(111) surface level, and the second smallest charge gain at the chlorine. These PACDD extremes for dimer 4 show that cooperatively controlled electron exchange

https://doi.org/10.1021/acs.jpcc.4c04678
J. Phys. Chem. C XXXX, XXX, XXX−XXX

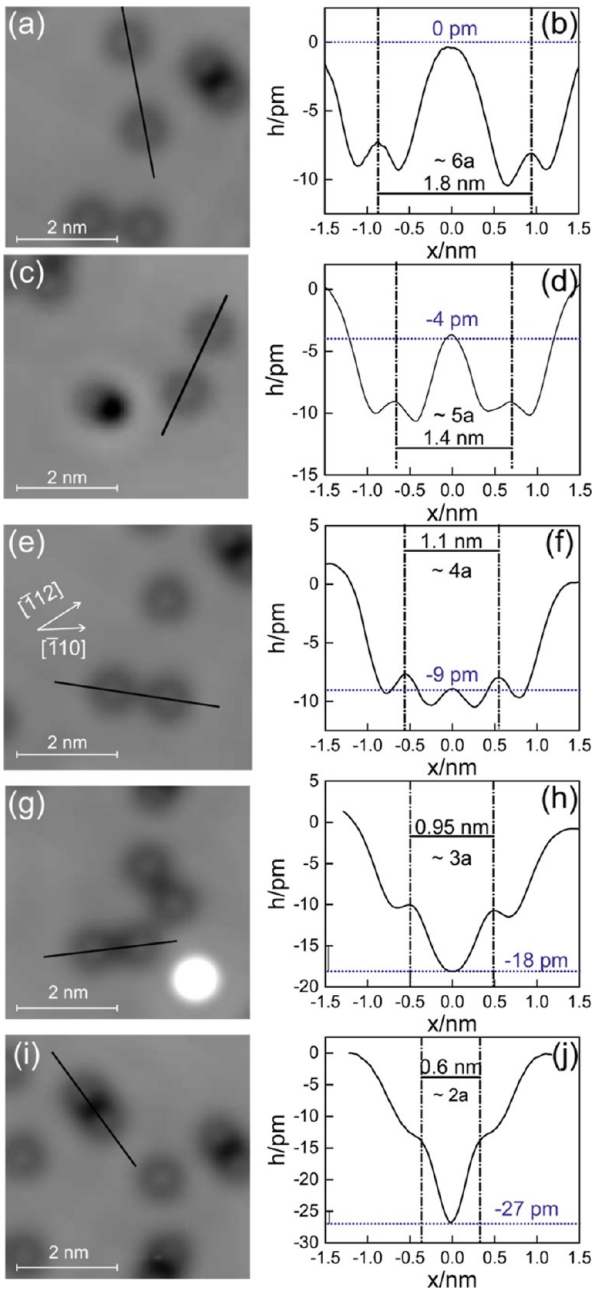

Figure 6. Interaction between dimers: (a,c,e,g,i) STM images and (b,d,f,h,j) apparent height profiles along the lines in the neighboring STM images at decreasing protrusion-to-protrusion distance: (a,b) 1.8, (c,d) 1.4, (e,f) 1.1, (g,h) 0.95, and (i,j) 0.6 nm; a = 0.289 nm is the lattice constant of Ag(111); the sample was prepared by one pulse from the ALI system; the images were recorded at 936 mV and 270 pA.

between the surface and adsorbate is important for stabilizing these chlorines and the Ag(111) surface. Thus, the PACDD calculations support the cooperation of the chlorines for the charge transfer, visible in the STM images as a larger depression between the chlorines of a dimer or larger oligomers, for which the extraction of charge by chlorine increases (Figure 3j,k, red line). Moreover, the iCOHP clearly shows that dimer 4 has the strongest Ag−Cl bonding.

The different distances between the dimers led to their varying orientations, as observed experimentally. The distance of ≈0.5 nm at site 5 corresponds to the $\sqrt{3}$ distance between

Table 1. Chlorine Atom Average Bader Charges and Select Maximum and Minimum PACDD Values on the Ag(111) Surface for the Energetically Preferred Monomer, Various Dimer Site Options Referencing the Sites Possible from Figure 8a, Three Trimers of Different Geometry, a Pseudohexagonal Superstructure with Alternate Adsorption of Neighboring Chlorines in Positions 5 and 7 (5 + 7), and a Hexagonal Superstructure with Adsorption in Position 6 (6 + 6)

system	Cl Bader charge average (e)	PACDD max at Cl per Cl (e/nm)	PACDD min above Ag(111) per Cl (e/nm)	PACDD max below Ag(111) per Cl (e/nm)
monomer	−0.53	30.21	−64.12	15.23
dimer—pos. 1	−0.52	46.97	−76.70	14.24
dimer—pos. 2	−0.51	34.51	−65.78	15.27
dimer—pos. 3	−0.52	32.93	−67.03	15.47
dimer—pos. 4	−0.52	30.82	−63.85	15.95
dimer—pos. 5	−0.52	30.70	−65.05	15.74
dimer—pos. 6	−0.52	31.71	−65.59	15.71
dimer—pos. 7	−0.52	32.99	−67.15	15.71
trimer—linear	−0.51	31.61	−65.64	16.35
trimer—angled	−0.51	31.98	−65.34	16.19
trimer—triangular	−0.51	31.90	−64.82	16.20
superstr. (5 + 7)	−0.49	34.30	−67.15	17.14
superstr. (6 + 6)	−0.49	35.38	−67.11	17.22

equivalent hollow sites in a ⟨112⟩ direction in the energetically preferred $\sqrt{3} \times \sqrt{3}$ $R30°$ superstructure, and the distance in site 6 is 2a, twice the lattice constant, to the energetically similar (2 × 2) superstructure.[13] The dimer orientations are reflected in the symmetry of these superstructures.

The bimodal distance distribution of chlorines within trimers of various shapes and orientations peaks at (0.46 ± 0.02) nm (58% of the values) and (0.53 ± 0.02) nm (25%), suggesting a preference for sites 4 and 5. Theory predicts that trimers and tetramers with the adjacent chlorines in site 4 are energetically preferred (see Supporting Information). The alternation between the fcc and hcp site for oligomers with chlorines in sites 4 explains the zigzag appearance of the trimers and tetramers (Figure 3g−i). The orientation of the calculated oligomers follows the ⟨110⟩ surface directions, as in experiment. The chlorine−chlorine interaction, thus, over-compensates the slight preference for fcc hollow site adsorption.

There is an abundance of dimers, while trimers are rare. We here define dimers and trimers as interacting chlorines, indicated by the reduced apparent height on the surface between them, while pairs or trios are in a smaller distance than expected from a random distribution, determined visually, without a reduced apparent height. Only 12.6% of more than 1400 chlorines are trimers, i.e., three chlorines close enough that the apparent height of the surface between them is reduced. 4.7% are within trios, three chlorines in a proximity that resulted from a single precursor due to their distance within a radius of 3 nm. More chlorines are monomers, at 29.9%. Most chlorines are either in dimers, at 38.5%, or pairs, at 13.0%, two chlorines with an apparent height of the surface value between them. Very few chlorines (1.3%) are within the larger oligomers. The statistics suggests that either chloroform mainly releases two chlorines, leading to dimers, or the chlorines are highly mobile at the adsorption temperature, such

https://doi.org/10.1021/acs.jpcc.4c04678
J. Phys. Chem. C XXXX, XXX, XXX−XXX

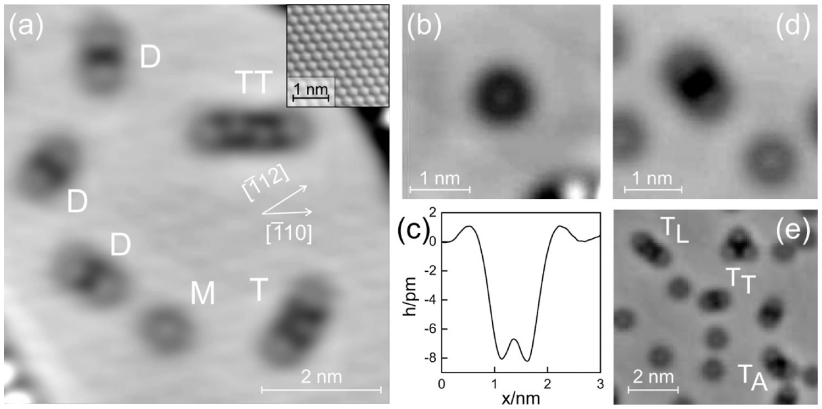

Figure 7. Oligomers at submonolayer coverage: (a) overview image with monomer M, dimers D, trimer T, and tetramer TT; inset: atomically resolved Ag(111) surface; (b) monomer (c) apparent height profile of monomer, (d) dimer (e) coexisting trimers; T_L, T_A, and T_T mark linear, angled, and triangular trimer, respectively; the images were recorded at (a) 210 mV, 30 pA, (b−d) 12 mV, 420 pA, and (e) 200 mV, 70 pA; inset in panel (a) at 8.4 mV, 4.2 nA.

Table 2. Adsorption Site, Adsorption Energy (E_{ads}) per Cl, Cl−Cl Interatomic Distance, and Ag−Cl Bonding Strength (iCOHP) per Cl for the Energetically Preferred Monomer, Various Dimer Site Options Referencing the Sites Possible from Figure 8a, Trimers of Different Geometry, a Pseudohexagonal Superstructure with Alternating Adsorption in Sites 5 and 7 between Neighboring Chlorines (5 + 7), and a Hexagonal Superstructure with Neighboring Chlorines in Adsorption Site 6 (6 + 6); the Values in Square Brackets Refer to the Next Nearest Neighboring Distances

system	adsorption site	E_{Ads} per Cl (eV)	Ag−Cl iCOHP per Cl (eV/Cl)	Cl−Cl distance (nm)
monomer	fcc	−3.317	−6.380	
dimer—pos. 1	fcc-top/hcp-top	−3.084	−3.185	0.338
dimer—pos. 2	fcc-bridge/fcc-bridge	−3.302	−4.855	0.368
dimer—pos. 3	fcc/hcp	−3.306	−6.305	0.387
dimer—pos. 4	fcc/hcp	−3.348	−6.470	0.445
dimer—pos. 5	fcc/fcc	−3.332	−6.440	0.504
dimer—pos. 6	fcc/fcc	−3.330	−6.445	0.590
dimer—pos. 7	fcc/hcp	−3.321	−6.385	0.615
trimer—linear	fcc/hcp	−3.326	−6.502	0.448/0.450 [0.880]
trimer—angled	fcc/hcp	−3.347	−6.519	0.449/0.449 [0.774]
trimer—triangular	fcc/hcp	−3.360	−6.554	0.448/0.449 [0.586]
superstructure (5 + 7)	fcc/hcp	−3.499	−6.685	0.512/0.611 [0.688]
superstructure (6 + 6)	fcc	−3.361	−6.728	0.591

that they easily move to form thermodynamically preferred structures. For kinetically limited dimers, we recall that the dissociative adsorption of CCl_4 on Ag(111) at room temperature leads to chemisorbed chlorine on the surface accompanied by the desorption of tetrachloroethylene (C_2Cl_4).[5] Thereby, C_2Cl_4 forms from two carbene precursors, CCl_2, after two chlorine atoms have been dissociated from CCl_4. The reason is likely a considerably stronger C−Cl bond of the carbene than the C−Cl bonds of the intact molecule. Based on the chemical and physical similarity of CCl_4 and $CDCl_3$, the dissociative adsorption of $CDCl_3$ is expected to lead largely to dimers or pairs of chlorine atoms accompanied by the desorption of 1,2-dichloroethene formed by combining two CDCl carbene precursors. Such a product is expected to desorb from the Ag(111) surface at room temperature. On the other hand, dimers are preferred thermodynamically over monomers and trimers (Table 2). The combined adsorption energies of four monomers or a monomer with a linear trimer are, at 13.268 and 13.358 eV, respectively, less favorable than those of two dimers, at 13.392 eV. Moreover, we calculated that the transition state energy for a chlorine diffusing from a fcc to a hcp site through a bridge site is about 0.1 eV, an energy that is easily surmountable at room temperature. The rather low energetic barrier supports chlorine mobility and diffusion along the Ag(111) surface between hollow sites as necessary to form oligomers. Thus, dimers are thermodynamically and kinetically the preferred species at low chlorine coverages from chloroform dissociation.

Having understood the direct interaction of the chlorines, we now turn to higher oligomers. Meandering chains at higher submonolayer coverage extend the oligomers observed at lower coverage (Figure 9a). The adjacent chlorines along the linear structures are thereby also slightly displaced from the ⟨110⟩ directions of the surface (lines in Figure 9b). Their connecting line approximately dissects the ⟨110⟩ and ⟨112⟩ directions, consistent with the direction of adsorption site 4. It clearly rules out adsorption site 5, for which neighboring chlorines were oriented along one of the ⟨112⟩ directions. Larger structures occasionally change their directions. It reflects that other trimer configurations (T_A, T_L, T_T) are similar in energy (Table 2).

At higher coverage, the linear structures coalesce into a porous structure, supporting second-layer islands already at a submonolayer coverage (Figure 10a). Higher density compresses the porous structure to a pseudohexagonal layer embedded in the quasi-linear network (Figure 10b−d). The

https://doi.org/10.1021/acs.jpcc.4c04678
J. Phys. Chem. C XXXX, XXX, XXX−XXX

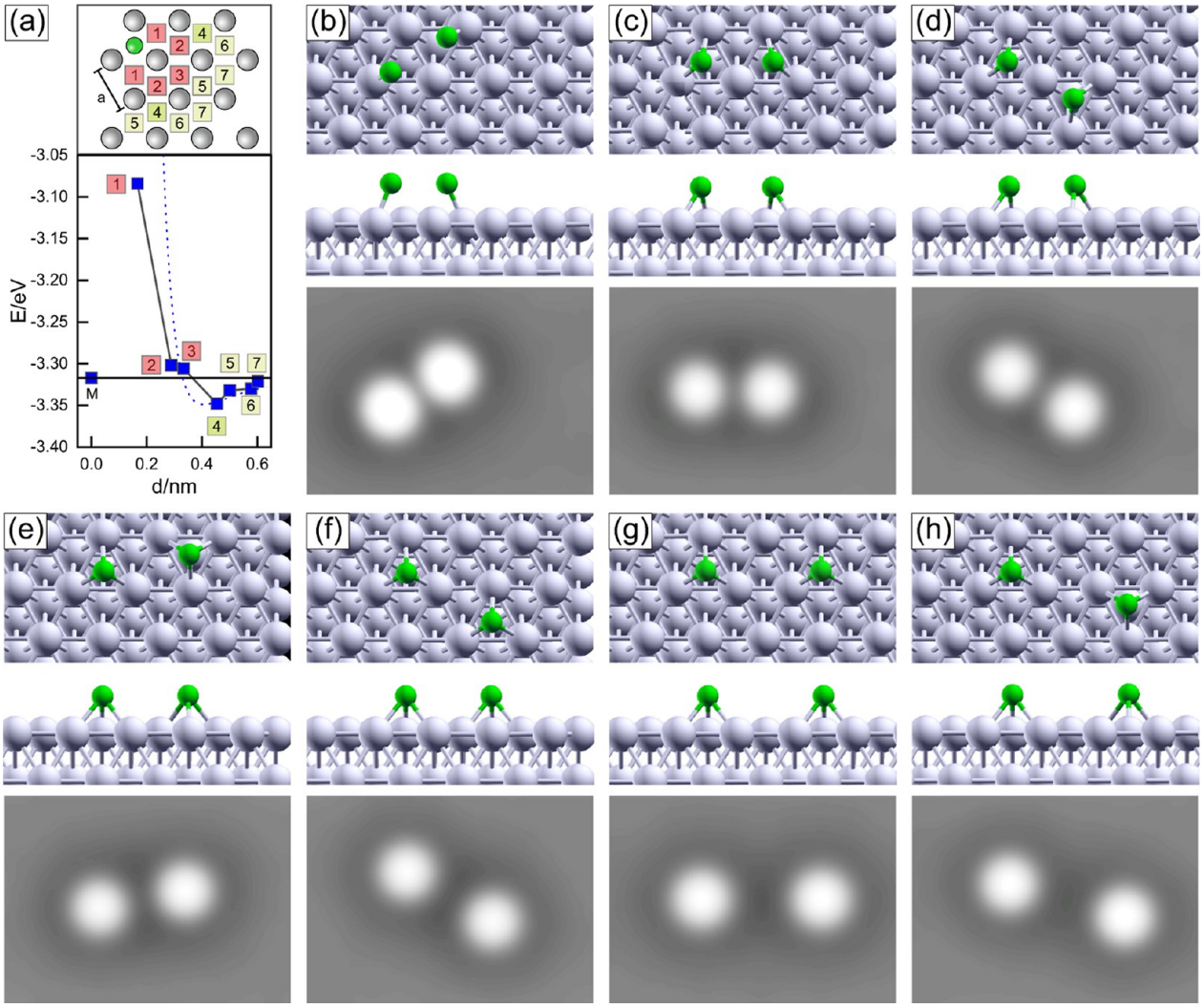

Figure 8. Chlorine dimers: (a) adsorption energy of dimers E vs the adsorption-site distance d referenced to the monomer adsorption site (at d = 0) and energy (horizontal line); a Lennard-Jones 12−6 potential is approximated as a dotted line; top: scheme of chlorine adsorption sites: boxes number the seven closest 3-fold hollow sites relative to the chlorine (green ball) on Ag(111) (gray balls); red (green) squares mark distances that are repulsive (attractive) compared to two separated monomers with dark green the preferred adsorption site 4; (b−h) optimized structures of dimers in adsorption sites 1 (b), 2 (c), 3 (d), 4 (e), 5 (f), 6 (g), and 7 (h) according to the definition in panel (a).

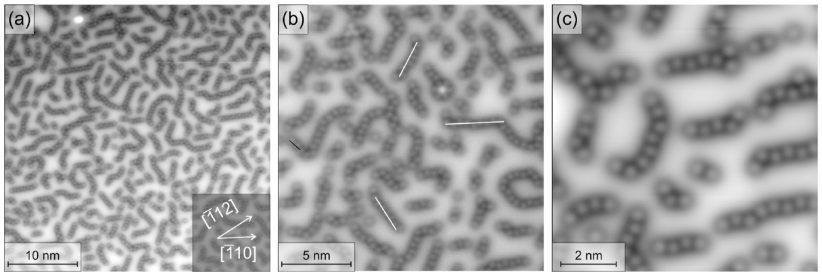

Figure 9. Linear chlorine structures at submonolayer coverage: (a) large-scale STM image; (b) medium-scale STM image; lines mark ⟨110⟩ surface directions; (c) small-scale STM image; the sample was prepared by one pulse from the ALI system; the images were recorded at (a,b) 6.2 pA, 60 mV and (c) 12 pA, 64 mV.

chlorine rows follow one of the Ag⟨110⟩ directions. There is no obvious deviation from a straight line in the pseudohexagonal structure pointing to other relative adsorption sites of neighboring chlorines than for the oligomers. The distance between the chlorines in the pseudohexagonal structures varies between 0.51 nm and 0.62 nm, consistent with sites 5 and 7 (Figure 10b−d). Indeed, the energetically preferred superstructure consists of alternating distances of 5 and 7 between the individual chlorines (Figure 10e,f). Its rectangular unit cell with two base atoms corresponds to a pseudohexagonal superstructure (Figure 10e,f, rectangles). The pseudohexagonal superstructure is the most favorable structure energetically of all chlorine structures observed because of its strong Ag−Cl bonding according to the iCOHP (Table 2), along with the

https://doi.org/10.1021/acs.jpcc.4c04678
J. Phys. Chem. C XXXX, XXX, XXX−XXX

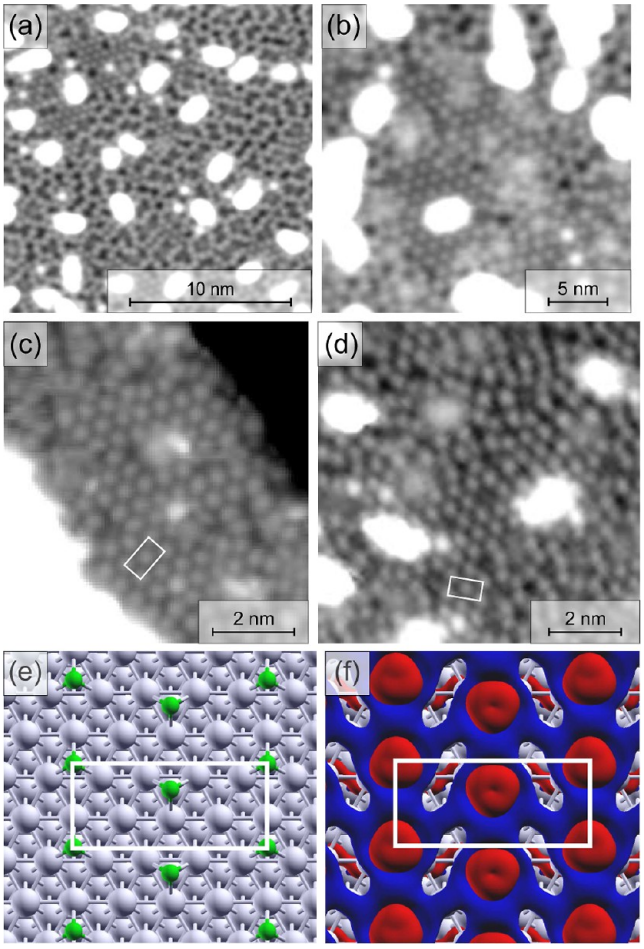

Figure 10. Chlorine layer at higher submonolayer coverage: (a) large-scale image; (b) medium-scale image; (c,d) small-scale images; (e) optimized pseudohexagonal superstructure; (f) CDD plot of (e) at an isovalue of ±5 e/nm^3; the rectangles mark the rectangular primitive unit cells; the sample was prepared by five pulses from the ALI system; the images were recorded at (a) 13 pA, −254 mV, (b) 13 pA, 255 mV, (c) 60 pA, 553 mV, and (d) 13 pA, 498 mV.

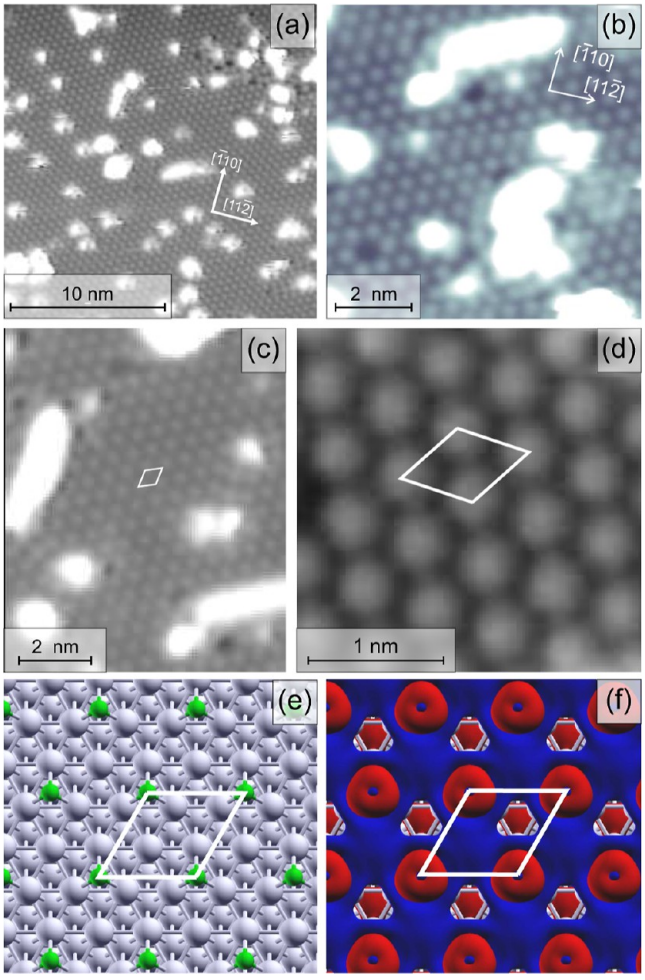

Figure 11. Chlorine superstructure in a full monolayer: (a) large-scale STM image; (b,c) medium-scale STM images; (d) small-scale STM image; (e) optimized hexagonal superstructure; (f) CDD plot of (e) at an isovalue of ±5 e/nm^3; rhombi mark hexagonal primitive unit cells; the samples were prepared by three to ten pulses from the ALI system; the images were recorded at (a−c) 24 pA, 200 mV and (d) 9.8 pA, −213 mV.

most efficient charge transfer from the silver to the chlorines, as calculated in the PACDD minimum (−67.15 e/nm, Table 1).

In an even more condensed hexagonal layer, the chlorine−chlorine distances are identical in the three directions, e.g., (0.54 ± 0.01) nm (Figure 11a) or (0.55 ± 0.03) nm (Figure 11b−d), in the range of two lattice constants at sites 6 of Ag(111). The experimental hexagonal arrangement is better reflected in the highly symmetric calculated superstructure with the chlorines in the distance of site 6 and a hexagonal unit cell (Figure 11e,f). It is comparable in energy to the superstructure with alternating distances corresponding to sites 5 and 7 (Table 2). The (2 × 2) superstructure has, at one chlorine per four surface atoms, a lower density than the thermodynamically slightly preferred $\sqrt{3} \times \sqrt{3}$ $R30°$ superstructure, at one chlorine per three surface atoms, but it is within the broad range of possible superstructures with very comparable energies formed at lower temperature.[13]

Both superstructures are more stable energetically relative to any of the other oligomers and structures modeled according to adsorption energy per Cl, PACDD values, and iCOHP (Tables 1 and 2). The iCOHP continually grows from the monomer to the dimer, to the trimer, and to the superstructure, detailing stronger and stronger Ag−Cl bonding strength. The chlorine atoms gain higher stabilization with increasing coverage due to the Ag−Cl interaction becoming more and more refined in its charge density transfer and Ag−Cl interaction strength improving by approximately 0.31 eV/Cl from the monomer to the superstructure. The PACDD demonstrates improved charge transfer and ionic interaction (Figure 3k, blue and purple lines). Its maximum at chlorine rises from monomer to dimer to trimer to superstructure. However, the calculated dipole per chlorine decreases as coverage increases from the monomer to the dimer to the trimer to the pseudohexagonal superstructure. It supports a decrease in Bader charge with increasing coverage. The superstructure differs from the dimer 4 and the trimer because it packs through site 5 instead of site 4. Note that already tetramers forming through site 4 destabilize relative to the trimer and dimer. It suggests that site 4 does not support larger chlorine structures, while sites 5 and beyond do.

The superstructure formation of chlorine differs from those of other hexagonal superstructures on metal surfaces. For

https://doi.org/10.1021/acs.jpcc.4c04678
J. Phys. Chem. C XXXX, XXX, XXX−XXX

neutral species, atoms, or molecules, superstructures often self-assemble already at low coverages in two-dimensional domains.[43] For cationic species, a hexagonal superstructure maximizes the cation−cation distance, such that the superstructure is highly coverage-dependent, decreasing at increasing coverages, e.g., for Cs on Cu(111),[17,44] in stark contrast to the one-dimensional structures formed here.

CONCLUSIONS

We have investigated the formation of a chlorine superstructure on Ag(111) from chloroform via chemical vapor deposition at room temperature from individual chlorines to a hexagonal monolayer. A substantial charge transfer from the silver surface to individual chlorine atoms, revealed in the differences in charge density, is reflected in a sombrero shape in the STM image. Despite their charge, oligomers are already formed at submonolayer coverage. A pronounced cooperative effect sets in for dimers, two monomers at a distance of 1 nm or below. The cooperative effect results from an improved interaction of chlorines in close proximity with Ag(111) while limiting electrostatic repulsion between the negatively charged chlorines. Thus, chlorines in close proximity improve the stability through enhancing the surface−adsorbate interaction. Varying distances between the dimers led to their varying orientations. Their preferred distance is 0.45 nm, with closer distances being repulsive. Despite the shorter oligomers being the most stable submonolayer species, an interaction asymmetry leads to longer linear oligomers connecting to a porous network at higher coverage. A hexagonal network forms only at (local) full layer coverage. In this network, the preferred distances between the chlorines are slightly larger than in the dimers or oligomers, between 0.5 nm and 0.6 nm, balancing electrostatic repulsion while keeping a strong Ag−Cl interaction. Theory suggests that both a pseudohexagonal (with alternating distances between neighboring chlorines) and a true hexagonal (2 × 2) superstructure (with the same distance) are both minima on the potential energy surface. This formation of a hexagonal superstructure from one-dimensional filaments differs from the more conventional condensation of adsorbates, in particular circular ones, into domains that merge into a monolayer at higher coverage. Moreover, the superstructure, grown from supersaturation at room temperature, is less dense than the thermodynamically preferred $\sqrt{3} \times \sqrt{3}$ $R30°$ superstructure.[13] As the chlorine density determines its charge state, this result is relevant for reactions involving chlorines on silver surfaces.

On a broader scale, understanding how chlorine-containing molecules interact with metal surfaces could help to develop chlorine absorbers to reduce pollution by the environmentally unfriendly chlorines that are contained in a variety of popular solvents, e.g., CCl_4, $CHCl_3$, CH_2Cl_2, and CH_3Cl.

ASSOCIATED CONTENT

Supporting Information

The Supporting Information is available free of charge at https://pubs.acs.org/doi/10.1021/acs.jpcc.4c04678.

Computational results for adsorption of the monomer, dimer, trimer, tetramer, and superstructure; adsorption of $CHCl_3$, $CDCl_3$, H, D, D_2, and H_2 on Ag(111); Ag−Cl and Cl−Cl iCOHPs and iCOOPs of chlorine adsorption structures; coordinates (VASP POSCAR format); and simulated STM images (PDF)

AUTHOR INFORMATION

Corresponding Authors

Daniel P. Miller − *Department of Chemistry, Hofstra University, Hempstead, New York 11549, United States;* orcid.org/0000-0003-1507-2667; Email: Daniel.P.Miller@hofstra.edu

Karina Morgenstern − *Physical Chemistry I, Universitätsstr. 150, Ruhr-Universität Bochum, D-44801 Bochum, Germany;* orcid.org/0000-0002-6660-5286; Email: karina.morgenstern@rub.de

Authors

Ivan Soldo − *Physical Chemistry I, Universitätsstr. 150, Ruhr-Universität Bochum, D-44801 Bochum, Germany*

Paul Schweer − *Physical Chemistry I, Universitätsstr. 150, Ruhr-Universität Bochum, D-44801 Bochum, Germany*

Marvin Quack − *Physical Chemistry I, Universitätsstr. 150, Ruhr-Universität Bochum, D-44801 Bochum, Germany*

Nico Knüfer − *Physical Chemistry I, Universitätsstr. 150, Ruhr-Universität Bochum, D-44801 Bochum, Germany*

David Olivenza − *Physical Chemistry I, Universitätsstr. 150, Ruhr-Universität Bochum, D-44801 Bochum, Germany;* orcid.org/0000-0002-2922-7722

Complete contact information is available at: https://pubs.acs.org/10.1021/acs.jpcc.4c04678

Notes

The authors declare no competing financial interest.

ACKNOWLEDGMENTS

This work was supported by the Research Training Group 'Confinement-Controlled Chemistry', funded by the Deutsche Forschungsgemeinschaft (DFG)—GRK2376/331085229. Funded by the Deutsche Forschungsgemeinschaft (DFG, German Research Foundation) under Germany's Excellence Strategy—EXC 2033−390677874—RESOLV and through the individual grant DFG 960/27-1. This article is based upon work from the COST Action CA21101—Confined Molecular Systems: From a New Generation of Materials to the Stars (COSY), supported by COST (European Cooperation in Science and Technology). We thank the National Science Foundation for support through grant CNS-2320735.

REFERENCES

(1) Serafin, J. G.; Liu, A. C.; Seyedmonir, S. R. Surface Science and the Silver-Catalyzed Epoxidation of Ethylene: an Industrial Perspective. *J. Mol. Catal. A: Chem.* **1998**, *131*, 157−168.

(2) Rovida, G.; Paretsi, I. Chlorine Monolayers on the Low-Index Faces of Silver. *Surf. Sci.* **1975**, *51*, 270−282.

(3) Goddard, P. J.; Lambert, R. M. Adsorption-Desorption Properties and Surface Structural Chemistry of Chloride on Cu(111) and Ag(111). *Surf. Sci.* **1977**, *67*, 180−194.

(4) Dixon-Warren, S. J.; Jensen, E. T.; Polanyi, J. C. Direct Evidence for Charge-Transfer Photodissociation at a Metal Surface: CCl_4/Ag(111). *Phys. Rev. Lett.* **1991**, *67*, 2395−2398.

(5) Bovet, N.; Sayago, D. I.; Allegretti, F.; Kröger, E.; Knight, M. J.; Barrett, J.; Woodruff, D. P.; Jones, R. G. The Adsorption of CCl_4 on Ag(111): Carbene and C = C Bond Formation. *Surf. Sci.* **2006**, *600*, 241−248.

(6) Petrova, N. V.; Yakovkin, I. N.; Braun, O. M. Lateral Interaction and Structures in Cl Adlayers on the Ag(111) Surface. *Chem. Phys.* **2011**, *383*, 35−40.

(7) Bowker, M.; Waugh, K. C. The Adsorption of Chlorine and Chloridation of Ag(111). *Surf. Sci.* **1983**, *134*, 639−664.

(8) Andryushechkin, B. V.; Eltsov, K. N.; Shevlyuga, V. M.; Yurov, V. Y. Atomic Structure of Saturated Chlorine Monolayer on Ag(111) Surface. *Surf. Sci.* **1998**, *407*, L633−L639.
(9) Andryushechkin, B. V.; Cherkez, V. V.; Gladchenko, E. V.; Zhidomirov, G. M.; Kierren, B.; Fagot-Revurat, Y.; Malterre, D.; Eltsov, K. N. Atomic Structure of Ag(111) Saturated with Chlorine: Formation of Ag_3Cl_7 Clusters. *Phys. Rev. B: Condens. Matter Mater. Phys.* **2011**, *84*, 075452.
(10) Andryushechkin, B. V.; Cherkez, V. V.; Gladchenko, E. V.; Zhidomirov, G. M.; Kierren, B.; Fagot-Revurat, Y.; Malterre, D.; Eltsov, K. N. Structure of Chlorine on Ag(111): Evidence of the (3 × 3) Reconstruction. *Phys. Rev. B: Condens. Matter Mater. Phys.* **2010**, *81*, 205434.
(11) Andryushechkin, B. V.; Cherkez, V. V.; Kierren, B.; Fagot-Revurat, Y.; Malterre, D.; Eltsov, K. N. Commensurate-Incommensurate Phase Transition in Chlorine Monolayer Chemisorbed on Ag(111): Direct Observation of Crowdion Condensation into a Domain-Wall Fluid. *Phys. Rev. B: Condens. Matter Mater. Phys.* **2011**, *84*, 205422.
(12) Shard, A. G.; Dhanak, V. R. Chlorine Adsorption on Silver (111) at Low Temperatures. *J. Phys. Chem. B* **2000**, *104*, 2743−2748.
(13) Gava, P.; Kokalj, A.; de Gironcoli, S.; Baroni, S. Adsorption of Chlorine on Ag(111): no Subsurface Cl at Low Coverage. *Phys. Rev. B: Condens. Matter Mater. Phys.* **2008**, *78*, 165419.
(14) Doll, K.; Harrison, N. M. Theoretical Study of Chlorine Adsorption on the Ag(111) Surface. *Phys. Rev. B: Condens. Matter Mater. Phys.* **2001**, *63*, 165410.
(15) Migani, A.; Illas, F. A Systematic Study of the Structure and Bonding of Halogens on Low-Index Transition Metal Surfaces. *J. Phys. Chem. B* **2006**, *110*, 11894−11906.
(16) Diehl, R. D.; McGrath, R. Current Progress in Understanding Alkali Metal Adsorption on Metal Surfaces. *J. Phys.: Condens. Matter* **1997**, *9*, 951−968.
(17) von Hofe, T.; Kröger, J.; Berndt, R. Adsorption Geometry of Cu(111)-Cs Studied by Scanning Tunneling Microscopy. *Phys. Rev. B: Condens. Matter Mater. Phys.* **2006**, *73*, 245434.
(18) Thomas, J.; Bertram, C.; Daru, J.; Patwari, J.; Langguth, I.; Zhou, P.; Marx, D.; Morgenstern, K.; Bovensiepen, U. Competition between Coulomb and van der Waals Interactions in Xe-Cs^+ Aggregates on Cu(111) Surfaces. *Phys. Rev. Lett.* **2021**, *127*, 266802.
(19) Schunke, C.; Miller, D. P.; Zurek, E.; Morgenstern, K. Halogen and Structure Sensitivity of Halobenzene Adsorption on Copper Surfaces. *Phys. Chem. Chem. Phys.* **2022**, *24*, 4485−4492.
(20) Lucht, K.; Ulrich, I.; Sander, W.; Morgenstern, K. Selectivity of Laser-Induced versus IET-Induced Carbene Formation from Methoxydiazofluorene on Ag(111). *J. Phys. Chem. C* **2023**, *127*, 562−567.
(21) Chen, B. W.; Kirvassilis, D.; Bai, Y.; Mavrikakis, M. Atomic and Molecular Adsorption on Ag(111). *J. Phys. Chem. C* **2019**, *123*, 7551−7566.
(22) Dixon-Warren, S. J.; Jensen, E. T.; Polanyi, J. C. Photochemistry of Adsorbed Molecules. XI. Charge-Transfer Photodissociation and Photoreaction in Chloromethanes on Ag(111). *J. Chem. Phys.* **1993**, *98*, 5938−5953.
(23) Kresse, G.; Furthmüller, J. Efficient Iterative Schemes for ab Initio Total-Energy Calculations Using a Plane-Wave Basis Set. *Phys. Rev. B: Condens. Matter Mater. Phys.* **1996**, *54*, 11169−11186.
(24) Klimes, J.; Bowler, D. R.; Michaelides, A. Chemical Accuracy for the van der Waals Density Functional. *J. Phys.: Condens. Matter* **2010**, *22*, 022201.
(25) Klimes, J.; Bowler, D. R.; Michaelides, A. Van der Waals Density Functionals Applied to Solids. *Phys. Rev. B: Condens. Matter Mater. Phys.* **2011**, *83*, 195131.
(26) Blöchl, P. E. Projector Augmented-Wave Method. *Phys. Rev. B: Condens. Matter Mater. Phys.* **1994**, *50*, 17953−17979.
(27) Kresse, G.; Joubert, D. From Ultrasoft Pseudopotentials to the Projector Augmented-Wave Method. *Phys. Rev. B: Condens. Matter Mater. Phys.* **1999**, *59*, 1758−1775.
(28) Monkhorst, H. J.; Pack, J. D. Special Points for Brillouin-Zone Integrations. *Phys. Rev. B: Condens. Matter Mater. Phys.* **1976**, *13*, 5188−5192.
(29) Tersoff, J.; Hamann, D. R. Theory of the Scanning Tunneling Microscope. *Phys. Rev. B: Condens. Matter Mater. Phys.* **1985**, *31*, 805−813.
(30) Maintz, S.; Deringer, V. L.; Tchougreeff, A. L.; Dronskowski, R. LOBSTER: A Tool to Extract Chemical Bonding from Plane-Wave Based DFT. *J. Comput. Chem.* **2016**, *37*, 1030−1035.
(31) Dweydari, A. W.; Mee, C. H. B. Work Function Measurements on (100) and (110) Surfaces of Silver. *Phys. Status Solidi A* **1975**, *27*, 223−230.
(32) Zhou, X.-L.; White, J. M. Alkyl Halide Photochemistry on Ag(111): I. Ethyl Chloride. *Surf. Sci.* **1991**, *241*, 244−258.
(33) Zhou, X.-L.; Blass, P. M.; Koel, B. E.; White, J. M. Low Energy Electron Induced Chemistry: C_2H_5Cl on Ag(111). *Surf. Sci.* **1992**, *271*, 452−467.
(34) Zhukov, V.; Rendulic, K. D.; Winkler, A. Coadsorption of Hydrogen and Potassium on Silver Single Crystal Surfaces. *Vacuum* **1996**, *47*, 5−11.
(35) Gawronski, H.; Henzl, J.; Simic-Milosevic, V.; Morgenstern, K. Using a Chemical Concept for Reactivity for the Interpretation of STM Images of Physisorbed Molecules. *Appl. Surf. Sci.* **2007**, *253*, 9047−9053.
(36) Gawronski, H.; Henzl, J.; Simic-Milosevic, V.; Morgenstern, K. Erratum to "Using a Chemical Concept for Reactivity for the Interpretation of STM Images of Physisorbed Molecules. *Appl. Surf. Sci.* **2009**, *255*, 7109.
(37) Hofer, W. A.; Foster, A. S.; Shluger, A. L. Theories of Scanning Probe Microscopes at the Atomic Scale. *Rev. Mod. Phys.* **2003**, *75*, 1287−1331.
(38) Gustafsson, A.; Okabayashi, N.; Peronio, A.; Giessibl, F. J.; Paulsson, M. Analysis of STM Images with Pure and CO-Functionalized Tips: a First-Principles and Experimental Study. *Phys. Rev. B* **2017**, *96*, 085415.
(39) Lamble, G. M.; Brooks, R. S.; Ferrer, S.; King, D. A.; Norman, D. Surface Structural Determination for a Weakly Ordered and a Disordered Phase of Cl on Ag(111). *Phys. Rev. B: Condens. Matter Mater. Phys.* **1986**, *34*, 2975−2978.
(40) Davis, L. C.; Everson, M. P.; Jaklevic, R. C.; Shen, W. Theory of the Local Density of Surface States on a Metal: Comparison with Scanning Tunneling Spectroscopy of a Au(111) Surface. *Phys. Rev. B: Condens. Matter Mater. Phys.* **1991**, *43*, 3821−3830.
(41) Morgenstern, K.; Braun, K.-F.; Rieder, K. H. Surface-State Depopulation on Small Ag(111) Terraces. *Phys. Rev. Lett.* **2002**, *89*, 226801.
(42) Mehlhorn, M.; Morgenstern, K. Height Analysis of Amorphous and Crystalline Ice Structures on Cu(111) in Scanning Tunneling Microscopy. *New J. Phys.* **2009**, *11*, 093015.
(43) Yang, Y.; Wang, C. Hierarchical Construction of Self-Assembled Low-Dimensional Molecular Architectures Observed by Using Scanning Tunneling Microscopy. *Chem. Soc. Rev.* **2009**, *38*, 2576−2589.
(44) Thomas, J.; Patwari, J.; Langguth, I.; Penschke, C.; Zhou, P.; Morgenstern, K.; Bovensiepen, U. Femtosecond Electron Transfer Dynamics Across the $D_2O/Cs^+/Cu(111)$ Interface: the Impact of Hydrogen Bonding. *J. Phys. Chem. C* **2023**, *127* (48), 23467−23474.

https://doi.org/10.1021/acs.jpcc.4c04678
J. Phys. Chem. C XXXX, XXX, XXX−XXX